3-2014

The DrrAB system of Streptomyces peucetius is a Multi-Drug Transporter of Broad Substrate Specificity

Wen Li
Georgia State University, pupaliwen@gmail.com

Madhu Sharma
Georgia State University

Parjit Kaur
Georgia State University, pkaur@gsu.edu

Recommended Citation

The DrrAB system of Streptomyces peucetius is a Multi-Drug Transporter of Broad Substrate Specificity. Wen Li, Madhu Sharma and Parjit Kaur. J. Biol. Chem. published online March 14, 2014. doi: http://dx.doi.org/10.1074/jbc.M113.536136

JBC Papers in Press. Published on March 14, 2014 as Manuscript M113.536136
The latest version is at http://www.jbc.org/cgi/doi/10.1074/jbc.M113.536136

The DrrAB system of *Streptomyces peucetius* is a Multi-Drug Transporter of Broad Substrate Specificity

Wen Li, Madhu Sharma and **Parjit Kaur

Department of Biology
Georgia State University
161 Jesse Hill Jr. Dr, Atlanta, GA-30303

*Running Title: DrrAB is a Multi-drug Transporter

To whom correspondence should be addressed: Parjit Kaur, Department of Biology, Georgia State University, 161 Jesse Hill Jr. Dr, Atlanta, GA-30303, Tel.:(404) 413-5405; E-mail: pkaur@gsu.edu

Keywords: Single-drug transporter, Multi-drug transporter, ABC transporter, Inside-out membrane vesicles, Drug binding sites, Competitive inhibition, Non-competitive inhibition

Background: DrrAB is dedicated to export of doxorubicin in *Streptomyces peucetius*, an organism which produces this anticancer drug. Whether this prototype system can export other drugs has not been investigated.
Results: DrrAB exports multiple drugs efficiently.
Conclusion: Substrate specificity of DrrAB overlaps with known bacterial and human multi-drug resistance proteins.
Significance: This study suggests common mechanisms and origin for DrrAB and other MDR proteins.

ABSTRACT

The soil bacterium *Streptomyces peucetius* produces two widely used anticancer antibiotics doxorubicin and daunorubicin. Present within the biosynthesis gene cluster in *S. peucetius* is the *drrAB* operon which codes for a dedicated ABC-type transporter for the export of these two closely related antibiotics. Because of its dedicated nature, the DrrAB system is believed to belong to the category of single-drug transporters. However, whether it also contains specificity for other known substrates of multidrug transporters has never been tested. In this study, we demonstrate under both *in vivo* and *in vitro* conditions that the DrrAB system can transport not only doxorubicin but is also able to export two most commonly studied MDR substrates, Hoechst 33342 and ethidium bromide. Moreover, we demonstrate that many other substrates (including verapamil, vinblastine, and rifampicin) of the well-studied multi-drug transporters inhibit DrrAB-mediated Dox transport with high efficiency, indicating that they are also substrates of the DrrAB pump. Kinetic studies show that inhibition of doxorubicin transport by Hoechst 33342 and rifampicin occurs by a competitive mechanism whereas verapamil inhibits transport by a non-competitive mechanism, thus suggesting the possibility of more than one drug binding site in the DrrAB system. This is the first in-depth study of a drug resistance system from a producer organism, and it shows that a dedicated efflux system like DrrAB contains specificity for multiple drugs. The significance of these findings in evolution of poly-specificity in drug resistance systems is discussed.

Multidrug resistance (MDR) has emerged as a major clinical problem in recent years both for the treatment of infectious diseases and for chemotherapy of cancer. Although many different mechanisms for drug resistance are known, a common strategy consists of active efflux of drugs from the cells (1). Drug transporters are categorized into either single-drug efflux systems (which are specific for a drug or a group of drugs) or multi-drug efflux systems that exhibit a broad specificity and can transport structurally and functionally unrelated compounds. These proteins function as either primary active (belonging to the ATP Binding Cassette superfamily) or secondary active transporters (2). The phenomenon of multidrug resistance was first characterized in mammalian cancer cells, where exposure to

anticancer drugs was seen to result in over-expression of ABC-type efflux pumps, such as P-glycoprotein and MRP1 (2). These proteins have since been shown to transport hundreds of structurally unrelated compounds, including amphipathic anti-cancer drugs, peptides, and fluorescent dyes, etc., thus conferring MDR in cancer cells. MDR is also widespread among bacteria - the best known ABC family members include the bacterial proteins LmrA and LmrCD in *L. lactis*, Sav1866 in *S. aureus*, and MsbA in *E. coli*.

While most of the ABC proteins mentioned above have served as useful models to characterize and understand the basis of MDR (2,3), the most extensive biochemical analysis of the nature of multidrug specificity has been carried out with Pgp (4,5). Together the analyses carried out by many different groups suggested that Pgp contains a large drug binding chamber which can accommodate several drugs simultaneously. It was also suggested that the drug binding chamber in Pgp is lined by several trans-membrane (TM) helices, including TMs 4-6 in TMD1 and TMs 9-12 in TMD2 (4). Most recently, the crystal structure of Pgp confirmed many findings of the biochemical analysis and showed that Pgp indeed contains a large and flexible drug binding cavity made of mostly hydrophobic and aromatic residues (6). Different drugs were seen to interact with residues in different parts of the flexible cavity, mostly through hydrophobic interactions, thus providing an explanation for the poly-specific nature of Pgp. The crystal structure of Pgp also revealed that some drugs were bound to a single site, while some others bound to two different locations within the cavity. The drug binding cavity of Pgp was found to reside within the cell membrane, and it showed the presence of two portals formed by TMs 4 and 6 and TMs 10 and 12 which allow direct entry of hydrophobic molecules from the membrane (6). This observation supports previous models, which proposed that Pgp can extract drugs directly from the lipid bilayer and remove them by a hydrophobic vacuum cleaner mechanism (7). The crystal structure of another MDR protein, AcrB, a secondary-active transporter, is also available. This structure also showed the presence of a very large central drug binding cavity, which could accommodate several ligand molecules simultaneously (8). However, the drug binding cavity, though present in the membrane, was found to be accessible to the periplasmic domain. Thus, in contrast to Pgp (where the drug portals are located in the membrane), the periplasmic region of AcrB seems to play a major role in determining substrate specificity, suggesting differences between the mechanisms of different MDR proteins.

The bacterial ABC drug transporters that have also been studied in significant detail include the *E. coli* ABC transporter MsbA (responsible for export of Lipid A, the core moiety of LPS), *L. lactis* homologue LmrA and *S. aureus* Sav1866 (3,9,10). All of these proteins have been shown to transport multiple drugs. Interestingly, MsbA was found to contain overlapping substrate specificity with LmrA and Sav1866 (11). Some newly identified members, such as VcaM from Non-O1 *Vibrio cholerae* and the YccC (BmrA) from *Bacillus subtilis* were also shown to transport multiple drugs (12,13). Therefore, a significant progress has indeed been made in understanding the phenomenon of multidrug resistance. However, the available information is based on the analysis of only a handful of drug transporters described above. Most other annotated drug transporters, especially those found in the antibiotic/drug producer organisms, have not been analyzed for their ability to confer MDR. Moreover, not much is known about why and how the ability to confer multidrug resistance evolves.

In this study, we analyzed the ABC transporter DrrAB, which confers self-resistance to two related anticancer antibiotics doxorubicin (Dox) and daunorubicin (Dnr) in the producer soil organism *Streptomyces peucetius*. The genes for this system are present in an operon located within the gene cluster for biosynthesis of Dox and Dnr, therefore they code for a dedicated transporter for these antibiotics. The DrrAB system represents the simplest form of an ABC drug transporter, which is assembled from two molecules each of DrrA (the catalytic subunit) and DrrB (integral membrane subunit) (14). In the mammalian Pgp, the two catalytic and two integral membrane domains are naturally fused into a single large polypeptide, possibly the result of an evolutionary gene fusion event (15). Both DrrAB and Pgp

confer resistance to the anticancer agents Dox and Dnr: DrrAB in the producer organism and Pgp in cancer cells. Therefore, the overall structure and function of the DrrAB transporter bears significant similarity to Pgp even though these two transporters belong to different classes of ABC proteins (16). Subcloning of the *drr*AB locus in *E. coli* was previously shown to confer doxorubicin resistance in this host (17). It was also previously shown that the DrrAB system confers resistance to Dox by an energy-dependent efflux mechanism (18). However, it is not known if this system is specific for Dox and Dnr, or if, like Pgp, it can also recognize and transport multiple drugs. Since this is a prototype drug resistance mechanism found in the producer organism, analysis of this system could shed light on the nature of substrate specificity and elucidate how the ability to confer multidrug resistance evolves in proteins.

In this paper, we provide in-depth characterization of drug transport by the DrrAB system and show that, contrary to the generally held assumption, this system forms a multidrug transporter. Using both *E. coli* whole cells and inside-out membrane vesicles (IOVs), it is shown that the DrrAB system can efficiently transport not only Dox, but also Hoechst 33342 (H 33342) and ethidium bromide (EtBr), two substrates most commonly used to establish the MDR phenotype (3,10,19). We also found that the DrrAB-mediated Dox efflux is inhibited by a number of other well-characterized MDR substrates, such as verapamil, rifampicin, vinblastine and colchicine, suggesting that these drugs are also substrates of the DrrAB pump. Interestingly, DrrAB-mediated efflux could be coupled to the energy of either ATP or GTP hydrolysis, and, as expected, the function of this transporter was found to be completely independent of the proton motive force (pmf). Since multiple drugs were found to inhibit Dox efflux by the DrrAB system, kinetics analysis was carried out to understand the mechanism of inhibition and interaction of drugs with DrrAB. Our studies revealed that inhibition of Dox efflux by H 33342 and rifampicin occurs by a competitive mechanism, whereas verapamil inhibits Dox transport by a non-competitive mechanism, suggesting that the DrrAB transporter may contain at least two drug binding sites. The findings of this paper demonstrate for the first time that the dedicated Dox transport system, DrrAB, can recognize and transport multiple drugs. This study highlights overlaps between the substrate specificity of the DrrAB system and Pgp and points to a common mechanism, and perhaps origin, for most MDR proteins.

EXPERIMENTAL PROCEDURES

Materials used – verapamil, vinblastine, rifampicin, doxorubicin hydrochloride, ethidium bromide, quinine, quinidine, colchicine, succinate, sodium fluoride, NADH (β-Nicotinamide adenine dinucleotide reduced disodium salt hydrate), ATP, GTP, and sodium *o*-vanadate were purchased from Sigma Aldrich. Hoechst 33342, rhodamine 123, rhodamine 6G, rhodamine B, and TMRM (Tetramethyl rhodamine) were obtained from Life Technology. Creatine kinase and creatine phosphate were purchased from Roche Diagnostics.

In vivo Dox efflux in cells – E. coli LE392Δ*uncIC* cells (Table 1) containing either vector pSU2718 or pDX101(pSU2718/*drrAB*) were grown in 200 ml TEA medium [50 mM triethanolamine HCl, pH 6.9, 15 mM KCl, 10mM $(NH_4)_2SO_4$, 1mM $MgSO_4$] supplemented with 0.5% (w/v) glycerol, 2.5 µg/ml thiamine, 0.5% (w/v) peptone and 0.15% (w/v) succinate to mid-log phase and induced with 0.1 mM IPTG for 1 hr. The harvested cells were washed twice and resuspended in 100 µl TEA buffer. 10 µl of the cell suspension from above was incubated in 3 ml of TEA medium containing 10 µM doxorubicin and 5 mM 2,4-dinitrophenol for 11 h at 37 °C. The loaded cells were washed twice with 0.1 mM MOPS buffer, pH 7.0 and resuspended in 3 ml of MOPS buffer containing 2 mM $MgSO_4$. The fluorescence spectra were recorded on an Alphascan-2 spectrofluorometer (Photon Technology International, London, Ontario, Canada). The excitation wavelength for doxorubicin was 480 nm, and emission was monitored at 590 nm. The excitation and emission slit widths were both set at 1.00 mm, and a time-based script was run. After an initial recording of fluorescence for 100 s at 37 °C, energy was provided in the form of either 20 mM glucose or 20 mM succinate, and recording was continued for an additional 400 s. The rate of Dox efflux was

determined from the slope in the steady-state range (300 s to 500 s). Where indicated, 10 mM sodium fluoride was added as inhibitor of ATP synthesis.

In vivo ethidium bromide efflux in cells – *E. coli* LE392Δ*uncIC* cells containing the indicated plasmid were grown, induced, and loaded with various concentrations (1 µM to 100 µM) of EtBr, as described above, except that the loading time used was 1 hr at 37 °C. The loaded cells were washed twice with 0.1 mM MOPS, pH 7.0 and resuspened in 3 ml MOPS buffer containing 2 mM $MgSO_4$. EtBr efflux from loaded cells was measured fluorometrically (exi, 500 nm; emi, 580 nm) on an Alphascan-2 spectrofluorometer (Photon Technology International). After 100 s, energy was provided in the form of 20 mM glucose. The recording was continued for additional 400 s. The rate of EtBr efflux was determined from the slope in the steady-state range (300 s to 500 s).

Preparation of inside-out membrane vesicles (IOVs) – *E. coli* LE392Δ*uncIC* cells containing indicated plasmids were grown in 1 L LB medium at 37 °C until mid-log phase and induced with 0.25 mM IPTG at 37 °C for 3 hr. The cells pellet was re-suspended in 20 ml 1xPBS buffer, pH 7.4 and lysed with French Press at 16,000 p.s.i. twice. The membrane fraction was prepared according to the previously published protocol (14), except that the membrane vesicles were washed twice with 20 ml 1xPBS buffer.

In vitro Dox efflux in IOVs and kinetic analysis – 250 µg IOVs were resuspended in 3 ml 1x PBS buffer, pH 7.4 supplemented with 0.1 mg/ml creatine kinase and 5 mM creatine phosphate. Dox was added to a final concentration of 1.0 µM, or as indicated. The fluorescence spectra were recorded on an Alphascan-2-spectrofluorometer with excitation wavelength of 480 nm and emission wavelength of 590 nm. The excitation and emission slit width were set to 1.00 mm and data were collected at 0.1-s intervals. After 100 s, the detection was paused, 1 mM Mg^{2+} and 1 mM ATP, pH7.5 were added into the reaction and the detection was continued for additional 400 s. Where indicated, ATP was substituted with 1 mM GTP or 5 mM NADH. The rate of Dox transport was determined from the slope of the initial linear range between 100 s and 200 s. To determine the kinetics of Dox transport, efflux was measured at a wide range of Dox concentrations (0.1 µM to 6 µM). The data were fitted by the Michaelis–Menten equation ($V = V_{max}[S]/(K_m) + [S]$) by Sigma Plot Kinetics software in Single-Substrate Format.

In vitro Hoechst 33342 Efflux in IOVs – The DrrAB-mediated efflux of H 33342 was studied in IOVs, as described above for Dox Efflux with some modifications. Briefly, 250 µg IOVs were resuspended in 3 ml 1x PBS buffer, pH 7.4 supplemented with 0.1 mg/ml creatine kinase and 5 mM creatine phosphate and various concentrations of H 33342 (0.1 µM to 2.5 µM). The excitation and emission wavelengths of H 33342 were 355 nm and 457 nm, respectively. The rate of H 33342 transport was determined from the initial slope of the linear range between100 s to 200 s.

Vanadate inhibition of Dox efflux in IOVs – 250 µg IOVs were resuspended in 3 ml 1x PBS buffer, pH 7.4 supplemented with 0.1 mg/ml creatine kinase, 5 mM creatine phosphate, 1 µM Dox, and various concentrations of sodium *o*-vanadate (0 µM – 100 µM). The measurement of Dox efflux was performed, as described above. The rate of Dox transport was determined from the slope of the linear range between 100 s and 200 s.

Determination of IC_{50} – 250 µg IOVs were resuspended in 3ml 1xPBS buffer, pH 7.4 supplemented with 0.1 mg/ml creatine kinase and 5 mM creatine phosphate, 1 µM Dox, and various concentrations of the inhibitory drug. The measurement of Dox efflux was performed, as described above. The rate of Dox transport was determined from the slope of the initial linear range between 100 s and 200 s. Designating the efflux rate of the sample without inhibitor as 1.0, the relative rate of each sample was calculated. The average data of three independent experiments were plotted by 'Scatter Plot with simple error bars' in Sigma Plot 11.0 software and fitted by the dynamic curve fit (equation: $y = ae^{-bx}$, x: concentration of inhibitor; y: relative rate). The IC_{50} value was determined based on the concentration of the drug that brings about 50% inhibition of the DrrAB-mediated Dox efflux at a Dox concentration of 1 µM.

Kinetics of Dox efflux inhibition by known MDR substrates – To study the kinetic inhibition

of Dox efflux by H 33342, four different concentrations of Dox (0.25, 0.5, 0.75 and 1.0 µM) were individually mixed with a fixed concentration of H 33342 in 1x PBS buffer containing 250 µg IOVs, 0.1 mg/ml creatine kinase and 5 mM creatine phosphate. In total, four different concentrations of H 33342 (0, 0.2, 0.6 or 0.8 µM) were studied. Similar assays were set up to study kinetics of Dox inhibition by different drugs. Initial rate of Dox transport was determined, as described above. The rate of Dox transport obtained with 1 µM Dox and 0 µM H 33342 (or another drug) was designated as 1.0. The relative rates were then calculated for each efflux curve, and the data were plotted by Lineweaver-Burk plot using SigmaPlot - Kinetics software in Single-Substrate/Single-Inhibitor Kinetics Format. The error bars represent three independent experiments. The type of inhibition was determined based on the AICc value (Akaikes Information Criterion corrected); lower AICc values correspond to better fits to the data.

Point Mutations in DrrA – Site-directed mutagenesis of the *drrA gene* was carried out by a QuikChange Multisite-directed mutagenesis kit (Stratagene, La Jolla, CA). Using pDX101 (pSU2718/*drrAB*) plasmid as the template, Gln197, located in the Switch motif of DrrA, was changed to Histidine. The resulting plasmid was named pDX101(Q197H). Another plasmid, generated by substituting Tyr198 to Arginine, was named pDX101(Y198R). Double mutations of Gln197Tyr198 to His197Arg198 and His197His198 were also created, and these plasmids were named pDX101(Q197H/Y198R; HR) and pDX101(Q197H/Y198H; HH). Other mutations used in this study were described previously (Table 1).

ATPase activity in IOVs - 7.5 µg IOVs expressing either wild type DrrAB or DrrAB with mutations in the Switch motif were incubated in 1 ml reaction mixture containing 50 mM MOPs, pH 7.5, 1mM dithiothreitol, 10µl PK/LDH enzyme (Sigma Aldrich), 5 mM ATP, 0.25 mM NADH (β-Nicotinamide adenine dinucleotide) and 1.25 mM PEP[phosphor(enol)pyruvic acid] at 37 ºC for 10 min, as described previously (20). The reaction was started by addition of 2.5 mM $MgCl_2$. The optical density at 340 nm was monitored for 10 min using Shimadzu UV1601 spectrophotometer and the UV probe 2. 20 Kinetics software. The slope of the linear portion of each curve (between 200 s and 400 s) was used to calculate ATPase activity. The activity of the control IOVs (without DrrAB) was subtracted from the activity of each test sample to obtain DrrAB-specific activity. Relative activity was then calculated by dividing the activity of each sample by the activity of the wild type sample.

RESULTS

Characterization of the DrrAB-mediated Dox efflux under in vivo and in vitro conditions – An *in vivo* assay for studying DrrAB-mediated Dox efflux was reported previously (18,21) and is shown in Fig. 1A. In this study, we established conditions to study DrrAB-mediated Dox efflux under *in vitro* conditions using *E. coli* inside out membrane vesicles (IOVs) (Fig. 1B). Both *in vivo* and *in vitro* assays utilize the fluorescent nature of Dox to measure efflux in *E. coli* LE392Δ*uncIC* cells (or IOVs). This strain of *E. coli* contains a deletion in the *unc* genes; as a result it is unable to carry out synthesis of ATP using proton gradients or establish a proton gradient by hydrolysis of ATP (22). Therefore, it is possible to establish conditions where only the proton motive force (pmf) or ATP is available as a source of energy (described below). Dox is fluorescent in solution, however its accumulation inside the cells results in quenching of its fluorescence and its efflux results in an increase in fluorescence intensity (23).

In vivo Dox efflux – The basic strategy for studying efflux under *in vivo* conditions consists of loading of the de-energized cells with Dox (18), followed by addition of an energy source, which is expected to result in efflux of Dox and an increase in its fluorescence (Fig. 1A). Under the conditions used in our experimental system, use of succinate as energy will generate only proton motive force while glucose will generate both pmf and ATP, therefore allowing us to discriminate between the energy sources used by the DrrAB system. The data in Fig. 1A compare the rate of Dox efflux in DrrAB-containing cells in the presence of glucose or succinate. *E.coli* LE392Δ*uncIC* cells (containing empty vector) were used as negative control in these experiments. Two conclusions can be made from the data shown in Fig. 1A. First, the rate of Dox efflux by the DrrAB-containing

cells in the presence of glucose is about 5-fold higher as compared to the rate in control cells (Fig. 1A.2, compare columns 1 and 4). A small increase in Dox efflux efficiency seen in control cells on addition of glucose is likely due to the action of one of the several MDR pumps known to be present in *E. coli* (1). Secondly, in contrast to glucose, use of succinate as energy showed no increase in fluorescence intensity in DrrAB-containing cells (Fig. 1A.1, curve 2; Fig. 1A.2, column 2), indicating that pmf does not support Dox efflux by the DrrAB proteins. Confirmation of these results was obtained by addition of sodium fluoride, a specific inhibitor of ATP synthesis by substrate-level phosphorylation, to DrrAB-containing cells in the presence of glucose. The data show a drastic reduction in Dox efflux by the DrrAB-containing cells (Fig. 1A.1, curve 3; Fig. 1A.2, column 3), resulting in the same background levels of efflux as seen with succinate (column 2). These studies show that doxorubicin efflux by the DrrAB pump is solely ATP-dependent, and pmf is not required for this process, thus highlighting similarities between DrrAB and other MDR proteins of the ABC superfamily (19,24,25).

In vitro Dox efflux – To understand the kinetics of Dox transport, an *in vitro* Dox efflux assay was optimized using inside-out membrane vesicles, as described under Methods. In this assay, the vesicles were mixed with Dox, and efflux was initiated by addition of ATP and Mg^{2+}. Because of the inverted nature of the IOVs, DrrAB-mediated efflux results in accumulation of Dox inside the vesicles which is seen as quenching of its fluorescence (Fig. 1B.1). The data in Fig. 1B.1 show that addition of ATP/Mg^{2+} first results in a rapid non-specific decrease in Dox fluorescence due to interaction between Dox and ATP (23). This quick phase is then followed by a slower rate of quenching, which corresponds to the DrrAB-dependent efflux in the vesicles. The initial rate of Dox efflux was therefore determined from the linear slope of the fluorescence spectra between 100 s and 200 s. As seen in Fig.1B.1 and 1B.2, Dox transport activity in vesicles containing DrrAB was found to be almost 12-fold higher as compared to the control vesicles prepared from cells containing vector alone (Fig. 1B.2, compare columns 1 and 4). Absence of either Mg^{2+} (column 2) or ATP (column 3) resulted in the failure of these vesicles to transport Dox. Use of NADH as an energy source also did not support Dox efflux (column 6), once again confirming that proton motive force is not used by the DrrAB proteins as a source of energy. Surprisingly, when GTP was used as an energy source instead of ATP, even higher transport activity was observed (column 5). Dox-dependent ATP and GTP binding to DrrA was shown previously (17). Together these data indicate that either ATP or GTP (and Mg^{2+}) can serve as a source of energy for the Dox transport function of DrrAB.

Kinetic Analysis of Dox efflux in vitro –To understand the kinetics of Dox efflux by the DrrAB system, efflux was analyzed (as shown in Fig. 1B.1) at a wide range of Dox concentrations. The initial rate (slope between 100 s-200 s) of each efflux curve was determined. Efficiency of Dox efflux was then calculated, as described under Methods and Figure Legends. The data were fitted to a hyperbola using the Michaelis-Menten equation (with an R^2 of 0.89), yielding an apparent K_m of 0.38 μM and V_{max} of 1003 (arbitrary units, a.u.) (Fig. 1C). These data showed a linear increase in the rate of Dox transport at concentrations ranging between 0.1 μM and 1 μM, which became saturated after 3μM. The Dox transport data could also be fitted equally well by the Hill equation; the implication of this finding is discussed later.

Inhibition of Dox transport activity by sodium o-vanadate – Vanadate (Vi) is a known inhibitor of the ATPase activity of ABC proteins (26-29). Since it functions as an analog of Pi, the ADP·Vi·Mg^{2+} complex is trapped in the ATP binding pocket after a single catalytic turnover, thus blocking further hydrolysis of ATP as well as drug transport. To determine if the DrrAB system is inhibited by vanadate, Dox transport was measured in IOVs in the absence or presence of increasing amounts of vanadate (5 μM to 100 μM). The data in Fig. 1D show that vanadate is a potent inhibitor of the Dox transport of DrrAB, with an IC_{50} = 11 μM. A complete inhibition of the Dox transport activity was seen at 100 μM vanadate. These data are consistent with the previously reported studies on the inhibitory effect of vanadate on Pgp and MsbA (28,30).

Point mutations in the nucleotide binding domain (NBD) of DrrA compromise Dox transport activity – The N-terminal nucleotide binding domain of DrrA contains a 200 amino acids long ABC cassette consisting of all the conserved motifs (Walker A, Walker B, Signature motif/C-loop, Q-loop, and the Switch motif/H-loop) involved in ATP binding and hydrolysis (Fig. 2A.1). We previously reported that mutations in the conserved residues of DrrA confer Dox sensitivity (31). Mutations in Walker A, as expected, also compromised ATP binding (31). Here we evaluated the effect of several mutations on DrrAB-mediated Dox efflux in IOVs. The data in Fig. 2B show that, as expected, single point mutations in Walker A (such as G44A, G44S or K47R), signature (S141R), or the Walker B (E165Q) motif of DrrA result in a drastic effect on Dox transport activity. Since the sequence of the Switch motif of DrrA is different from most other ABC proteins (Fig. 2A), this region was analyzed in greater detail, as described below. Most ABC proteins normally contain a highly conserved histidine residue in their Switch motif, followed by an arginine, histidine, or a lysine (Fig. 2A.1). The conserved histidine of the Switch motif and a conserved glutamate immediately following the Walker B motif (both are shown as highlighted areas in Fig. 2) are together believed to be critical for formation of the active sites in ABC proteins. Zaitseva *et al* recently proposed that these two residues together form a catalytic dyad which functions in substrate-assisted catalysis (32). However, despite the high conservation of these two residues in ABC proteins, deviations in the sequence of these motifs are sometimes seen. Most commonly, a glutamine replaces the histidine in the Switch motif and an aspartate replaces the glutamate in the Walker B region. When present (for example, in TAP1 and LmrC), these deviations are seen to result in asymmetrical ATP binding pockets with one site being catalytically non-functional (33,34). Interestingly, however, despite the presence of the non-canonical glutamine residue (Q197 followed by Y198, resulting in QY sequence) in the Switch motif of DrrA (and its close prokaryotic homologs, Fig. 2A.2), it is able to form a functional drug transporter with DrrB, as seen in Fig. 1. Note that the close eukaryotic homologs of DrrA most often contain an HH sequence in the Switch region (Fig. 2A.3), and both prokaryotic and eukaryotic homologs contain the conserved glutamate in the Walker B region (specifically E165 in DrrA) (Figs. 2A.2 and 2A.3)

Since histidine is conserved in the Switch of most ABC proteins, we wondered if the DrrAB transporter will become more efficient if Q197 is substituted with a histidine or if the QY sequence is changed to the commonly occurring sequence HR or HH. Surprisingly, we found that the Q197H mutation in DrrA produces a drastic effect on Dox efflux, however mutation of Y198 to Y198R retains about 35% Dox efflux function (Fig. 2C). Interestingly, a double mutation HR (Q197H/Y198R) also resulted in Dox transport activity of about 38% indicating that the second mutation partially masked the harmful effect of the Q197H single mutation (Fig. 2C). By contrast, the double mutation HH (Q197H/Y198H) exhibited extremely low Dox efflux (Fig. 2C). To understand the role of Q197 and Y198 in catalysis, the effect of the above-mentioned mutations on the ATPase activity of the DrrAB complex was determined. We found that while Q197H produces a drastic effect on ATPase activity, both HR and HH double mutations show significant ATPase activity (43% and 61%, respectively) (Figs. 2D and 2E), indicating that the second mutation in each case partially compensates for the negative effect of the Q197H mutation on catalysis. Overall the findings in Fig. 2 indicate that residues Q197 and Y198 in the Switch motif of DrrA function together and that the QY sequence works much better than the HH or HR sequence for the overall Dox efflux function of the DrrAB complex. Interestingly, the HH double mutant still exhibits 60% ATP hydrolysis activity, which suggests that either the QY or the HH sequence could participate in the formation of functional catalytic sites in DrrA. However, the HH allele seems to be defective in specific communication between DrrA and DrrB resulting in significantly reduced Dox efflux (less than 5%). Therefore the context in which the Switch motif functions in different ABC proteins may determine the nature of this motif. The conserved glutamate E165 present near the Walker B region in DrrA served as a control in these experiments. Analysis of the E165Q mutation showed a drastic effect on

both hydrolysis of ATP and Dox efflux (Figs. 2B-D), which is consistent with the critical role of this residue previously reported in literature (35). How a glutamine residue participates in the formation of functional ATP binding pockets in DrrA is still an open question. However, we can draw from the analogous situations present in other ATP/GTP-binding proteins (including RecA and H-ras p21) which contain a catalytic glutamine residue (Q194 in RecA and Q61 in H-ras p21) in their switch II domain in the position corresponding to Q197 in DrrA (36-38). The 3-d structures of RecA and H-ras indicate that these glutamines show similar interactions with the catalytic glutamate and γ phosphate of ATP to those seen with histidine in the ABC proteins, therefore suggesting that the glutamine functions in a manner similar to histidine in producing the overall conformation of the active site. This is consistent with our observation that either QY or HH sequence can indeed participate in formation of the catalytic sites in DrrA although the HH sequence is deficient in energy transduction. In summary, the analyses in Fig. 2 confirm that a functional nucleotide binding domain of DrrA is essential for Dox efflux by the DrrAB system. The analysis of the Switch mutations, in particular, also indicates that the *in vitro* efflux assay described here can provide a sensitive and a valuable approach for elucidating the role of critical residues in the catalytic and drug transport function of the DrrAB complex.

DrrAB-mediated Dox efflux is inhibited by multiple MDR substrates – To determine if the DrrAB transporter can recognize and bind other known MDR substrates, inhibition of Dox efflux by different drugs was investigated in IOVs. These assays were carried out at a wide range of the inhibitor concentrations while maintaining a constant concentration of Dox, as described under Methods (determination of IC_{50} values). The data in Fig. 3 show that many known MDR drugs, including H 33342 (Fig. 3A), verapamil (Fig. 3B), and rifampicin (Fig. 3C), inhibit DrrAB-mediated Dox efflux with high efficiency. The data in Fig 3, panel D, summarize the inhibitory effects of many different MDR substrates and indicate that the IC_{50} values vary dramatically for different substrates. For example, H 33342, vinblastine, verapamil and rifampicin show relatively low IC_{50} values, while much higher concentrations of EtBr, quinidine, and colchicine were required for the same level of inhibition. These data suggest that the DrrAB system has multiple substrates, which bind with varying affinities. However, whether these drugs bind to the same site, or if there are multiple drug binding sites, can't be ascertained from these data. To understand the nature of drug binding, kinetics of DrrAB-mediated Dox efflux was studied at multiple Dox concentrations in the presence of several concentrations of each inhibitory drug, which is described below.

Kinetics of Dox Inhibition by MDR drugs – The data in Fig. 1C showed that the rate of Dox efflux by DrrAB-containing IOVs increases linearly between 0.1 μM and 1 μM Dox concentration, therefore four evenly distributed concentrations of Dox within this range (0.25, 0.50, 0.75, and 1.0 μM) were used in the kinetics analysis. At each concentration of Dox, efflux was measured in the presence of our different concentrations of H 33342, verapamil, or rifampicin. These drugs were chosen based on their low IC_{50} values seen in inhibition studies (Fig.3D). (Since Dox and EtBr together were incompatible in the fluorescence-based assays due to their overlapping excitation/emission spectra, this combination could not be used in this study). The initial slope (100-200 seconds) for each Dox efflux curve was determined. The slope of the Dox efflux curve at 1.0 μM Dox and 0 concentration of the inhibitor was designated as 1, which was then used to calculate the relative slope of each curve obtained in the presence of the inhibitor, as described under Methods. The relative slopes were plotted by the Lineweaver-Burk plots using the Sigma Plot kinetics software (Fig. 4). The data in Fig. 4A indicate that the inhibition of Dox efflux by H 33342 is characteristic of competitive inhibition; the K_m of DrrAB-mediated Dox transport increased at increasing concentration of H 33342, whereas the V_{max} remained unchanged. These data suggest that Dox and H 33342 may bind to the same site in DrrAB. The apparent inhibition constant (Ki for H 33342) was found to be 0.64 μM, which corresponds well to the IC_{50} value of H 33342 (Fig 3, panel D). When studying the inhibition of Dox transport by rifampicin, a similar pattern was observed, which indicated a competitive inhibition between Dox

and rifampicin (Fig. 4C). However, the kinetics of inhibition of Dox transport by verapamil showed a different pattern (Fig. 4B). The V_{max} decreased at increasing concentration of verapamil, while K_m remained unaltered, indicating a non-competitive inhibition between Dox and verapmail. These data suggest that verapmail may bind to both the unliganded DrrAB and the binary DrrAB-Dox complex. The *K*i value for verapamil inhibition was found to be 9.4 μM, which also matches well to the IC_{50} of verapamil (Fig. 3, panel D). The observed competitive and non-competitive inhibitions of DrrAB-mediated Dox transport in IOVs imply that DrrAB must contain at least two drug binding sites.

The DrrAB system is a multidrug transporter – To determine whether the DrrAB system can actually transport other drugs in addition to Dox, two substrates (H 33342 and EtBr) commonly used to establish the MDR phenotype (10,19), were tested in IOVs, as described under Methods. In addition, five other fluorescent dyes or drugs (including Hoechst 34580, Hoechst 33258, quinine, TMRM, and Rhodmine 123) were also tested. Of these substrates, H 33342 and EtBr were successfully transported by the DrrAB system, as described below.

H 33342 is a cell-permeable dye, which is fluorescent only when bound to the cell membrane and loses its fluorescence in aqueous environment. Thus a decrease in fluorescence is expected when H 33342 is transported by the DrrAB system from the membrane to the inner aqueous environment in the IOVs. EtBr, on the other hand, becomes fluorescent when bound to DNA inside the cells. Therefore, DrrAB-mediated efflux of EtBr was studied in preloaded cells, as described under Methods. EtBr efflux under this condition is expected to result in quenching of fluorescence. The data in Fig. 5 show that both H 33342 (Fig 5A.1) and EtBr (Fig 5B.1) are transported efficiently by the DrrAB system. In the case of H 33342, the rate of transport was seen to decrease after an initial linear phase of transport. This is likely due to depletion of H 33342 in the membrane and due to passive rebinding of H 33342 to the membrane from the aqueous phase, as shown earlier in the case of Pgp (19). To determine the kinetic parameters for the transport of H 33342 and EtBr, efflux of each substrate was analyzed at a wide range of concentrations. The initial rate of H 33342 transport in DrrAB-containing IOVs was measured between 0.1 μM and 2.5 μM (Fig 5A.2). The efficiency of H 33342 transport was calculated, as described earlier for Dox (Fig. 1C). The data were plotted using the Michaelis-Menten equation by the Sigma Plot kinetics software and could be fitted to a hyperbola with an R^2 of 0.90, yielding an apparent K_m of 0.78 μM and V_{max} of 16000 (a.u.). To study kinetics of EtBr transport, energy-depleted cells were loaded with different concentrations of EtBr (ranging from 1 μM to 100 μM) for 1 hour, and efflux was initiated by addition of 20 mM glucose (Fig 5B.2). The data fitted to the hyperbola (Michaelis-Menten equation) with an R^2 of 0.97, yielding an apparent K_m of 21μM and V_{max} of 550 (a.u.). The data in Fig 5 show that both H 33342 and EtBr are transported efficiently by the DrrAB system. A comparison of the K_m and V_{max} values for transport of Dox, H 33342, and EtBr is shown in Fig 5, panel C. Five other fluorescent substrates (Hoechst 34580, Hoechst 33258, quinine, tetramethylrhodamine (TMRM), and Rhodmine 123) tested in this study were not found to be exported by the DrrAB system (data not shown). In general, the transport data agreed with the inhibition data shown in Fig. 3, panel D. Interestingly, of the three Hoechst dyes tested, only H 33342 was transported. Recent studies showed that a certain balance between the hydrophobic and hydrophilic forces in the structure of the target substrate is essential for optimum efflux by Pgp (39). Since H 33342 is the most amphiphilic of the three dyes, this may explain why DrrAB is able to preferentially transport H 33342 but not the other two dyes.

DISCUSSION

Multidrug resistance is conferred by the action of specialized proteins in the cell membrane that have the ability to carry out energy-dependent efflux of structurally and functionally unrelated hydrophobic compounds. This phenomenon defies the concept of single enzyme-single substrate (the lock and key model), which is applicable to most other enzymes. Since the discovery of multidrug resistance in human cancer cells and bacteria (40-42), two important questions have remained at the forefront of this field: 1) what is the basis of poly-specific drug recognition

and transport by MDR proteins? 2) How and why does MDR evolve? Extensive biochemical analysis of Pgp (1,4,5) as well as the availability of three-dimensional structures of the drug-bound forms of Pgp, AcrB, BmrR and QacR (6,8,43,44) has contributed significantly to understanding the molecular basis of poly-specific drug binding. These studies indicate that the MDR proteins contain an extensive (and flexible) drug binding pocket which can accommodate multiple drugs simultaneously via interactions with specific (sometimes overlapping) aromatic and polar residues present in different parts of the pocket. The 3-D structure of Pgp, in particular, also provides support for the hydrophobic vacuum cleaner model, which was proposed early on by Gottesman and colleagues (7,15) to explain the mechanism of multidrug transport. According to this model, Pgp substrates (which are primarily cationic, lipid soluble, planar molecules) partition spontaneously into the membrane and are picked up by Pgp directly from the membrane (instead of from the cytoplasm) and then removed by its ability to flip drugs from the inner to the outer leaflet. This model, which has now been extended to many other MDR proteins (45), makes a clear distinction between the classical solute transporters that remove molecules from an aqueous compartment and the MDR proteins that are proposed to function as flippases (46). A clear relationship between the ability of drugs to partition into the membrane and their binding and transport by Pgp has since been documented (47-49). Additional evidence in support of this model comes from 1) the ability of most MDR proteins studied to date to extrude the lipopilic dye H 33342 directly from the membrane (3,19,50,51), thus making it an ideal molecule to establish the MDR phenotype and 2) the ability of many MDR proteins to flip-flop lipids (52-55). Together, these observations led to the idea that hydrophobic drugs and lipids may use a common pathway or flipping mechanism for extrusion.

Despite significant progress in understanding the basis of poly-specific drug-binding, the origin of multidrug resistance still remains an enigma. It is generally accepted that most of the antibiotic and drug resistance genes found in clinical settings have their origins in the environmental bacteria (1). Indeed many antibiotic producing organisms contain dedicated export systems to protect themselves against their own antibiotics (56,57). Understanding these systems could hold the key to unraveling the origin and evolution of multidrug specificity. It is generally assumed that the dedicated systems found in producer organisms belong to the category of single-drug transporters as opposed to multi-drug transporters (2), however their substrate specificity has never been investigated in any significant detail thus providing the impetus for this study.

We show for the first time that the DrrAB system functions as a typical multidrug transporter that can carry out efflux of structurally unrelated substrates, including Dox, EtBr and H 33342. Inhibition studies further demonstrate that the substrate range of the DrrAB system includes many additional substrates, such as verapamil, vinblastine, and rifamicin, among others. Thus the substrate specificity of DrrAB overlaps with most other known MDR proteins, including Pgp (58-60). We found, however, that unlike Pgp, neither quinine nor rhodamine 123 serve as substrates for export by the DrrAB system nor did they show inhibition of Dox transport. Therefore, in spite of the broad substrate range of DrrAB, it appears that the range of substrates recognized by Pgp may still be larger (61), implying that the ability to bind some of these substrates may have evolved later in Pgp. Interestingly, the IC_{50} values varied significantly among different drugs, indicating the different binding affinities of each substrate. The highest IC_{50} was observed for colchicine, which is consistent with the data previously reported for Pgp (47,62,63). This may be related with low hydrophobicity of colchicines (64), therefore indicating that the ability to partition into the membrane may be an important factor for transport by both Pgp and DrrAB.

Kinetic characterization of Dox, H 33342, and EtBr transport by the DrrAB system revealed single-site transport kinetics. Further, the K_m values of 0.38 μM and 0.78 μM for transport of Dox and H 33342, respectively, reflect high affinity of these substrates for the DrrAB system and correspond well with the K_m values seen earlier for Dox transport by Pgp (65) and H 33342 transport by MsbA and LmrA (10). Interestingly, however, we found that the kinetic data for Dox as

well as H 33342 could also be fitted by the Hill equation (shown in Fig. 5C) providing the n_{Hill} value of 1.7 for Dox (R^2 = 0.93) and 2.0 for H 33342 (R^2 = 0.95), which suggests co-operative interaction between two or more drug binding sites in DrrAB. It is not clear from these data, however, whether both H 33342 and Dox bind to the same sites in the DrrAB system. Since EtBr transport by DrrAB exhibited only single-site transport kinetics (n_{Hill}=1.1; R^2 = 0.98) (Fig. 5C), it possibly interacts with only one of the Dox/Hoechst binding sites, or it may bind to a completely different site in DrrAB. The kinetic analyses shown in Fig. 4 provide evidence for competitive inhibition of Dox transport by H 33342 and rifampicin and non-competitive inhibition by verapamil. Therefore, we conclude that both H 33342 and rifampicin bind to the same site(s) as Dox, whereas verapamil may bind to a different site in DrrAB. Evidence for two or more non-identical drug binding sites has also been obtained previously with MsbA (10,53), LmrA (25) and Pgp (10,66,67). In Pgp, the two sites were defined as the H and R sites based on their preferential binding to H 33342 and Rhodamine, respectively (68). Together, these data point towards the presence of two or more drug binding sites in the DrrAB system. Gleaning from the knowledge previously gained from studies with Pgp and AcrB, these different drug binding sites are likely part of the same binding pocket in DrrB. However, in the absence of a crystal structure of the DrrAB transporter, this conclusion is only tentative.

Even though the present study does not provide an answer to the origin of poly-specific drug recognition, it does indeed show that a simple system like DrrAB (which may be closely related to the ancestral system) already contains the ability to recognize and transport multiple substrates. This leads us to conjecture that the ability to transport multiple drugs is an inherent property of a certain class of proteins that followed a different evolutionary path than the classical transporters. This work also opens new questions regarding the mechanism by which the DrrAB system extrudes multiple hydrophobic substrates. The most important of these questions is whether this system relies on a hydrophobic vacuum cleaner-like mechanism and if it is capable of flippase action? Doxorubicin is produced inside *S. peucetius* cells, therefore presumably the function of the DrrAB system is to remove it from the cytoplasmic compartment to the outside. Being amphipathic, however, Dox could conceivably partition into the cell membrane and then be picked up by the DrrB protein directly from the membrane, as suggested in an early model proposed for AcrB function (8). This strategy for its removal could also provide protection to the cell from the toxic effects of free Dox inside the cell. The ability to transport H 33342 no doubt indicates that the DrrB protein can indeed extract this fluorescent dye directly from the membrane by a mechanism similar to the one used by Pgp and other proteins (10,19,60). Future studies will therefore focus on an in-depth analysis of the mechanism of drug extrusion by the DrrAB system.

This and previous studies on MDR proteins raise many other intriguing questions; for example, is there evolutionary relatedness between MDR proteins and lipid flippases? What is the real difference between the single-drug and multi-drug transporters? What makes certain proteins specific for a substrate and some others multi-specific? What is the contribution of high aromatic amino acid content of the TM helices of MDR proteins in conferring poly-specificity? Since the transmembrane helices of Pgp and other MDR proteins, such as the bacterial BMR, are highly enriched in aromatic amino acids (18% and 15.4% for Pgp and BMR, respectively) as compared to the single-drug transporter TetA (9.4%), Pawagi et al. proposed that a greater number of aromatic amino acids may correlate with a decrease in substrate specificity of a transporter by providing additional binding sites for drugs containing aromatic rings in their structure (69). Moreover, it was shown that mutagenesis of a single residue Ser941 to Phe in TM11 of Pgp significantly altered its drug efflux profile (70). The recent 3-D structure confirmed that the drug-binding pocket of Pgp is made up of mostly hydrophobic and aromatic residues (6). Interestingly, we found that the aromatic amino acid content of predicted TM helices of DrrB (71) is also relatively high (15%) which is close to the aromatic content of Pgp (18%) and BMR (15.4%). Whether this plays a role in conferring multi-

specificity in DrrB will be determined in future studies by mutagenesis of specific aromatic and other residues in DrrB.

REFERENCES

1. Nikaido, H. (2009) Multidrug resistance in bacteria. *Annual Review of Biochemistry* **78**, 119-146
2. Lubelski, J., Konings, W. N., and Driessen, A. J. (2007) Distribution and physiology of ABC-type transporters contributing to multidrug resistance in bacteria. *Microbiology and Molecular Biology Reviews : MMBR* **71**, 463-476
3. Velamakanni, S., Yao, Y., Gutmann, D. A., and van Veen, H. W. (2008) Multidrug transport by the ABC transporter Sav1866 from Staphylococcus aureus. *Biochemistry* **47**, 9300-9308
4. Loo, T. W., and Clarke, D. M. (2005) Recent progress in understanding the mechanism of P-glycoprotein-mediated drug efflux. *The Journal of Membrane Biology* **206**, 173-185
5. Sharom, F. J. (2008) ABC multidrug transporters: structure, function and role in chemoresistance. *Pharmacogenomics* **9**, 105-127
6. Aller, S. G., Yu, J., Ward, A., Weng, Y., Chittaboina, S., Zhuo, R., Harrell, P. M., Trinh, Y. T., Zhang, Q., Urbatsch, I. L., and Chang, G. (2009) Structure of P-glycoprotein reveals a molecular basis for poly-specific drug binding. *Science* **323**, 1718-1722
7. Higgins, C. F., and Gottesman, M. M. (1992) Is the multidrug transporter a flippase? *Trends in Biochemical Sciences* **17**, 18-21
8. Yu, E. W., Aires, J. R., and Nikaido, H. (2003) AcrB multidrug efflux pump of Escherichia coli: composite substrate-binding cavity of exceptional flexibility generates its extremely wide substrate specificity. *Journal of Bacteriology* **185**, 5657-5664
9. van Veen, H. W., Venema, K., Bolhuis, H., Oussenko, I., Kok, J., Poolman, B., Driessen, A. J., and Konings, W. N. (1996) Multidrug resistance mediated by a bacterial homolog of the human multidrug transporter MDR1. *Proceedings of the National Academy of Sciences of the United States of America* **93**, 10668-10672
10. Woebking, B., Reuter, G., Shilling, R. A., Velamakanni, S., Shahi, S., Venter, H., Balakrishnan, L., and van Veen, H. W. (2005) Drug-lipid A interactions on the Escherichia coli ABC transporter MsbA. *Journal of Bacteriology* **187**, 6363-6369
11. Kerr, I. D., Jones, P. M., and George, A. M. (2010) Multidrug efflux pumps: the structures of prokaryotic ATP-binding cassette transporter efflux pumps and implications for our understanding of eukaryotic P-glycoproteins and homologues. *The FEBS Journal* **277**, 550-563
12. Huda, N., Lee, E. W., Chen, J., Morita, Y., Kuroda, T., Mizushima, T., and Tsuchiya, T. (2003) Molecular cloning and characterization of an ABC multidrug efflux pump, VcaM, in Non-O1 Vibrio cholerae. *Antimicrobial Agents and Chemotherapy* **47**, 2413-2417
13. Steinfels, E., Orelle, C., Fantino, J. R., Dalmas, O., Rigaud, J. L., Denizot, F., Di Pietro, A., and Jault, J. M. (2004) Characterization of YvcC (BmrA), a multidrug ABC transporter constitutively expressed in Bacillus subtilis. *Biochemistry* **43**, 7491-7502
14. Kaur, P., and Russell, J. (1998) Biochemical coupling between the DrrA and DrrB proteins of the doxorubicin efflux pump of Streptomyces peucetius. *The Journal of Biological Chemistry* **273**, 17933-17939
15. Gottesman, M. M., and Pastan, I. (1993) Biochemistry of multidrug resistance mediated by the multidrug transporter. *Annual Review of Biochemistry* **62**, 385-427
16. I. Barry Holland, S. P. C. C., Karl Kuchler and Christopher F. Higgins. (2003) *ABC Proteins: from Bacteria to Man*, Academic Press
17. Kaur, P. (1997) Expression and characterization of DrrA and DrrB proteins of Streptomyces peucetius in Escherichia coli: DrrA is an ATP binding protein. *Journal of Bacteriology* **179**, 569-575
18. Li, W., Rao, D. K., and Kaur, P. (2013) Dual role of the metalloprotease FtsH in biogenesis of the DrrAB drug transporter. *The Journal of Biological Chemistry* **288**, 11854-11864
19. Shapiro, A. B., Corder, A. B., and Ling, V. (1997) P-glycoprotein-mediated Hoechst 33342 transport out of the lipid bilayer. *European Journal of Biochemistry / FEBS* **250**, 115-121

20. Urbatsch, I. L., and Senior, A. E. (1995) Effects of lipids on ATPase activity of purified Chinese hamster P-glycoprotein. *Arch Biochem Biophys* **316**, 135-140
21. Zhang, H., Pradhan, P., and Kaur, P. (2010) The extreme C terminus of the ABC protein DrrA contains unique motifs involved in function and assembly of the DrrAB complex. *The Journal of Biological Chemistry* **285**, 38324-38336
22. Angov, E., and Brusilow, W. S. (1988) Use of lac fusions to measure in vivo regulation of expression of Escherichia coli proton-translocating ATPase (unc) genes. *Journal of Bacteriology* **170**, 459-462
23. Chambon, M. H., and Viratelle, O. M. (1998) Interaction of doxorubicin with ATP: quantification of complexes and effect on its diffusion into DNA-loaded liposomes--implication for ATP-driven transport studies. *Analytical Biochemistry* **263**, 198-207
24. Eckford, P. D., and Sharom, F. J. (2008) Functional characterization of Escherichia coli MsbA: interaction with nucleotides and substrates. *The Journal of Biological Chemistry* **283**, 12840-12850
25. van Veen, H. W., Margolles, A., Muller, M., Higgins, C. F., and Konings, W. N. (2000) The homodimeric ATP-binding cassette transporter LmrA mediates multidrug transport by an alternating two-site (two-cylinder engine) mechanism. *The EMBO Journal* **19**, 2503-2514
26. Taguchi, Y., Yoshida, A., Takada, Y., Komano, T., and Ueda, K. (1997) Anti-cancer drugs and glutathione stimulate vanadate-induced trapping of nucleotide in multidrug resistance-associated protein (MRP). *FEBS Letters* **401**, 11-14
27. Szabo, K., Szakacs, G., Hegeds, T., and Sarkadi, B. (1999) Nucleotide occlusion in the human cystic fibrosis transmembrane conductance regulator. Different patterns in the two nucleotide binding domains. *The Journal of Biological Chemistry* **274**, 12209-12212
28. Urbatsch, I. L., Sankaran, B., Weber, J., and Senior, A. E. (1995) P-glycoprotein is stably inhibited by vanadate-induced trapping of nucleotide at a single catalytic site. *The Journal of Biological Chemistry* **270**, 19383-19390
29. Sharma, S., and Davidson, A. L. (2000) Vanadate-induced trapping of nucleotides by purified maltose transport complex requires ATP hydrolysis. *Journal of Bacteriology* **182**, 6570-6576
30. Doerrler, W. T., and Raetz, C. R. (2002) ATPase activity of the MsbA lipid flippase of Escherichia coli. *The Journal of Biological Chemistry* **277**, 36697-36705
31. Rao, D. K., and Kaur, P. (2008) The Q-Loop of DrrA Is Involved in Producing the Closed Conformation of the Nucleotide Binding Domains and in Transduction of Conformational Changes between DrrA and DrrB. *Biochemistry* **47**, 3038-3050
32. Zaitseva, J., Jenewein, S., Jumpertz, T., Holland, I. B., and Schmitt, L. (2005) H662 is the linchpin of ATP hydrolysis in the nucleotide-binding domain of the ABC transporter HlyB. *The EMBO Journal* **24**, 1901-1910
33. Lubelski, J., van Merkerk, R., Konings, W. N., and Driessen, A. J. (2006) Nucleotide-binding sites of the heterodimeric LmrCD ABC-multidrug transporter of Lactococcus lactis are asymmetric. *Biochemistry* **45**, 648-656
34. Ernst, R., Koch, J., Horn, C., Tampe, R., and Schmitt, L. (2006) Engineering ATPase activity in the isolated ABC cassette of human TAP1. *The Journal of Biological Chemistry* **281**, 27471-27480
35. Moody, J. E., Millen, L., Binns, D., Hunt, J. F., and Thomas, P. J. (2002) Cooperative, ATP-dependent association of the nucleotide binding cassettes during the catalytic cycle of ATP-binding cassette transporters. *The Journal of Biological Chemistry* **277**, 21111-21114
36. Story, R. M., and Steitz, T. A. (1992) Structure of the recA protein-ADP complex. *Nature* **355**, 374-376
37. Pai, E. F., Krengel, U., Petsko, G. A., Goody, R. S., Kabsch, W., and Wittinghofer, A. (1990) Refined crystal structure of the triphosphate conformation of H-ras p21 at 1.35 A resolution: implications for the mechanism of GTP hydrolysis. *The EMBO Journal* **9**, 2351-2359

38. Frech, M., Darden, T. A., Pedersen, L. G., Foley, C. K., Charifson, P. S., Anderson, M. W., and Wittinghofer, A. (1994) Role of glutamine-61 in the hydrolysis of GTP by p21H-ras: an experimental and theoretical study. *Biochemistry* **33**, 3237-3244
39. Li-Blatter, X., Beck, A., and Seelig, A. (2012) P-glycoprotein-ATPase modulation: the molecular mechanisms. *Biophysical Journal* **102**, 1383-1393
40. Chen, C. J., Chin, J. E., Ueda, K., Clark, D. P., Pastan, I., Gottesman, M. M., and Roninson, I. B. (1986) Internal duplication and homology with bacterial transport proteins in the mdr1 (P-glycoprotein) gene from multidrug-resistant human cells. *Cell* **47**, 381-389
41. Cole, S. P., Bhardwaj, G., Gerlach, J. H., Mackie, J. E., Grant, C. E., Almquist, K. C., Stewart, A. J., Kurz, E. U., Duncan, A. M., and Deeley, R. G. (1992) Overexpression of a transporter gene in a multidrug-resistant human lung cancer cell line. *Science* **258**, 1650-1654
42. Doyle, L. A., Yang, W., Abruzzo, L. V., Krogmann, T., Gao, Y., Rishi, A. K., and Ross, D. D. (1998) A multidrug resistance transporter from human MCF-7 breast cancer cells. *Proceedings of the National Academy of Sciences of the United States of America* **95**, 15665-15670
43. Schumacher, M. A., Miller, M. C., Grkovic, S., Brown, M. H., Skurray, R. A., and Brennan, R. G. (2001) Structural mechanisms of QacR induction and multidrug recognition. *Science* **294**, 2158-2163
44. Heldwein, E. E., and Brennan, R. G. (2001) Crystal structure of the transcription activator BmrR bound to DNA and a drug. *Nature* **409**, 378-382
45. Poelarends, G. J., Mazurkiewicz, P., and Konings, W. N. (2002) Multidrug transporters and antibiotic resistance in Lactococcus lactis. *Biochimica et Biophysica Acta* **1555**, 1-7
46. Borst, P., Zelcer, N., and van Helvoort, A. (2000) ABC transporters in lipid transport. *Biochimica et Biophysica Acta* **1486**, 128-144
47. Seelig, A., and Landwojtowicz, E. (2000) Structure-activity relationship of P-glycoprotein substrates and modifiers. *European journal of pharmaceutical sciences : Official Journal of the European Federation for Pharmaceutical Sciences* **12**, 31-40
48. Romsicki, Y., and Sharom, F. J. (1999) The membrane lipid environment modulates drug interactions with the P-glycoprotein multidrug transporter. *Biochemistry* **38**, 6887-6896
49. Omote, H., and Al-Shawi, M. K. (2006) Interaction of transported drugs with the lipid bilayer and P-glycoprotein through a solvation exchange mechanism. *Biophysical Journal* **90**, 4046-4059
50. Shapiro, A. B., and Ling, V. (1997) Positively cooperative sites for drug transport by P-glycoprotein with distinct drug specificities. *European Journal of Biochemistry / FEBS* **250**, 130-137
51. Mazurkiewicz, P., Driessen, A. J., and Konings, W. N. (2004) Energetics of wild-type and mutant multidrug resistance secondary transporter LmrP of Lactococcus lactis. *Biochimica et Biophysica Acta* **1658**, 252-261
52. Eckford, P. D., and Sharom, F. J. (2005) The reconstituted P-glycoprotein multidrug transporter is a flippase for glucosylceramide and other simple glycosphingolipids. *The Biochemical Journal* **389**, 517-526
53. Siarheyeva, A., and Sharom, F. J. (2009) The ABC transporter MsbA interacts with lipid A and amphipathic drugs at different sites. *The Biochemical Journal* **419**, 317-328
54. Margolles, A., Putman, M., van Veen, H. W., and Konings, W. N. (1999) The purified and functionally reconstituted multidrug transporter LmrA of Lactococcus lactis mediates the transbilayer movement of specific fluorescent phospholipids. *Biochemistry* **38**, 16298-16306
55. Romsicki, Y., and Sharom, F. J. (2001) Phospholipid flippase activity of the reconstituted P-glycoprotein multidrug transporter. *Biochemistry* **40**, 6937-6947
56. Tahlan, K., Ahn, S. K., Sing, A., Bodnaruk, T. D., Willems, A. R., Davidson, A. R., and Nodwell, J. R. (2007) Initiation of actinorhodin export in Streptomyces coelicolor. *Molecular Microbiology* **63**, 951-961

57. Blanc, V., Salah-Bey, K., Folcher, M., and Thompson, C. J. (1995) Molecular characterization and transcriptional analysis of a multidrug resistance gene cloned from the pristinamycin-producing organism, Streptomyces pristinaespiralis. *Molecular Microbiology* **17**, 989-999
58. Rautio, J., Humphreys, J. E., Webster, L. O., Balakrishnan, A., Keogh, J. P., Kunta, J. R., Serabjit-Singh, C. J., and Polli, J. W. (2006) In vitro p-glycoprotein inhibition assays for assessment of clinical drug interaction potential of new drug candidates: a recommendation for probe substrates. *Drug metabolism and disposition: the biological fate of chemicals* **34**, 786-792
59. Parveen, Z., Stockner, T., Bentele, C., Pferschy, S., Kraupp, M., Freissmuth, M., Ecker, G. F., and Chiba, P. (2011) Molecular dissection of dual pseudosymmetric solute translocation pathways in human P-glycoprotein. *Molecular Pharmacology* **79**, 443-452
60. Putman, M., Koole, L. A., van Veen, H. W., and Konings, W. N. (1999) The secondary multidrug transporter LmrP contains multiple drug interaction sites. *Biochemistry* **38**, 13900-13905
61. Sharom, F. J. (2007) *Multidrug resistance protein: P-glycoprotein. in Drug Transporters: Molecular Characterization and Role in Drug Disposition*, John Wiley & Sons, Inc., Hoboken, NJ, USA.
62. Safa, A. R., Glover, C. J., Sewell, J. L., Meyers, M. B., Biedler, J. L., and Felsted, R. L. (1987) Identification of the multidrug resistance-related membrane glycoprotein as an acceptor for calcium channel blockers. *The Journal of Biological Chemistry* **262**, 7884-7888
63. Safa, A. R. (1988) Photoaffinity labeling of the multidrug-resistance-related P-glycoprotein with photoactive analogs of verapamil. *Proceedings of the National Academy of Sciences of the United States of America* **85**, 7187-7191
64. Doige, C. A., and Sharom, F. J. (1992) Transport properties of P-glycoprotein in plasma membrane vesicles from multidrug-resistant Chinese hamster ovary cells. *Biochimica et Biophysica Acta* **1109**, 161-171
65. Awasthi, S., Singhal, S. S., Srivastava, S. K., Zimniak, P., Bajpai, K. K., Saxena, M., Sharma, R., Ziller, S. A., 3rd, Frenkel, E. P., Singh, S. V., and et al. (1994) Adenosine triphosphate-dependent transport of doxorubicin, daunomycin, and vinblastine in human tissues by a mechanism distinct from the P-glycoprotein. *The Journal of Clinical Investigation* **93**, 958-965
66. Martin, C., Berridge, G., Higgins, C. F., Mistry, P., Charlton, P., and Callaghan, R. (2000) Communication between multiple drug binding sites on P-glycoprotein. *Molecular Pharmacology* **58**, 624-632
67. Ayesh, S., Shao, Y. M., and Stein, W. D. (1996) Co-operative, competitive and non-competitive interactions between modulators of P-glycoprotein. *Biochimica et Biophysica Acta* **1316**, 8-18
68. Shapiro, A. B., and Ling, V. (1998) The mechanism of ATP-dependent multidrug transport by P-glycoprotein. *Acta Physiologica Scandinavica. Supplementum* **643**, 227-234
69. Pawagi, A. B., Wang, J., Silverman, M., Reithmeier, R. A., and Deber, C. M. (1994) Transmembrane aromatic amino acid distribution in P-glycoprotein. A functional role in broad substrate specificity. *Journal of Molecular Biology* **235**, 554-564
70. Gros, P., Dhir, R., Croop, J., and Talbot, F. (1991) A single amino acid substitution strongly modulates the activity and substrate specificity of the mouse mdr1 and mdr3 drug efflux pumps. *Proceedings of the National Academy of Sciences of the United States of America* **88**, 7289-7293
71. Gandlur, S. M., Wei, L., Levine, J., Russell, J., and Kaur, P. (2004) Membrane topology of the DrrB protein of the doxorubicin transporter of Streptomyces peucetius. *The Journal of Biological Chemistry* **279**, 27799-27806

Acknowledgement **-** We thank Giovanni Gadda for help with analysis of the kinetics data.

FOOTNOTES

*This work was supported in part by a National Institutes of Health Service Award RO1 GM51981-09 to P.K.

**To whom correspondence should be addressed: Department of Biology, Georgia State University, 161 Jesse Hill Jr. Dr, Atlanta, GA-30303, Tel.:(404) 413-5405; E-mail: pkaur@gsu.edu

The abbreviations used are: Dox, doxorubicin; Dnr, daunorubicin; H 33342, Hoechst 33342; EtBr, ethidium bromide; MDR, multidrug resistance; ABC, ATP Binding Cassette; Pgp, P-glycoprotein; IOVs, inside-out membrane vesicle; pmf, proton motive force; Vi, vanadate; NBD, Nucleotide Binding Domain

FIGURE LEGENDS

FIGURE 1. Characterization of the DrrAB-mediated Dox efflux under *in vivo* and *in vitro* conditions. (A) *In vivo* analysis of DrrAB-mediated Dox efflux using *E. coli* cells. *E. coli* LE392*ΔuncIC* cells containing either vector or pDX101 (DrrAB) were loaded with 10 µM Dox, and the whole cell Dox efflux assay was performed, as described under Methods and in ref (21). Dox efflux was measured fluorometrically (exi, 480 nm; emi, 590 nm) on an Alphascan-2 spectrofluorometer (Photon Technology International). Energy was provided in the form of 20 mM glucose or 20 mM succinate at 100 seconds (marked with an arrow) and fluorescence was monitored for an additional 400 seconds. 10 mM sodium fluoride (NaF) was added to the samples, where indicated. **A.1:** Curve 1, pDx101(DrrAB)/glucose; Curve 2, pDx101 (DrrAB)/succinate; Curve 3, pDx101 (DrrAB)/glucose/NaF; Curve 4, pSU2718 (vector)/glucose; Curve 5, pSU2718/succinate; Curve 6, pSU2718/glucose/NaF. **A.2: Quantitative presentation of the Dox efflux data shown in Fig 1A.1.** The slope of the linear portion of each curve shown in Fig 1A.1 was calculated. The slope of curve 1 was designated as 1.0. Relative slope of each curve was then obtained by dividing the slope of the curve by the slope of curve 1. The average data obtained from three independent experiments are shown in the histogram. **(B) *In vitro* analysis of DrrAB-mediated Dox efflux using inside-out membrane vesicles (IOVs).** *E. coli* LE392*ΔuncIC* cells containing either vector or pDX101 (DrrAB) were grown to mid-log phase and induced with 0.25 mM IPTG at 37 °C for 3 hr. The membrane fraction was prepared (14) and Dox efflux in DrrAB-containing IOVs was performed, as described under Methods. **B.1:** *In vitro* Dox efflux assay was carried out using 250 µg IOVs in the presence of 1 µM Dox, 0.1 mg/ml creatine kinase and 5 mM creatine phosphate in 3 ml PBS buffer, pH 7.5, as described under Methods. Vector, Dox efflux in IOVs prepared from cells containing empty vector; DrrAB, Dox efflux in IOVs prepared from cells containing pDX101 (DrrAB). **B.2: Quantitative presentation of Dox efflux in DrrAB-containing IOVs under various conditions.** *In vitro* Dox efflux assay was carried out in the presence or absence of 1 mM ATP, 1mM GTP, 1 mM Mg or 5 mM NADH, as described under Methods. The initial rate of Dox efflux was determined from the linear slope of the fluorescence spectra between 100 s and 200 s. The slope of the efflux curve obtained by incubation of the DrrAB-containing IOVs with ATP and Mg^{2+} (column 4) was designated as 1.0. The relative slope for each curve was then calculated by dividing the slope of the curve by the slope of sample 4. The average data obtained from three independent experiments are shown in the histogram. **(C) Kinetic analysis of DrrAB-mediated Dox efflux in IOVs.** *In vitro* Dox efflux was analyzed using 250 µg IOVs in the presence of increasing concentrations of Dox (0.1 µM to 6.0 µM) and 1 mM ATP/Mg^{2+}. The initial linear rate of Dox efflux was determined for each curve. The data obtained from three independent experiments were fitted to the Michaelis-Menten equation and plotted by SigmaPlot-Kinetics software using the equation for Single Substrate Format. **(D) Inhibition of DrrAB-mediated Dox efflux by sodium *o*-vanadate.** *In vitro* Dox efflux was measured using 250 µg IOVs in the presence 1 µM Dox, 1 mM ATP and 1 mM Mg^{2+} and increasing concentrations of Vi (0 – 100 µM). The initial slope of the efflux curve obtained with 0 µM Vi was designated as 1.0. The relative slope of each curve was

determined, as described under panel A.2. The average data obtained from three independent experiments are shown in the histogram.

FIGURE 2. Effect of point mutations in the NBD of DrrA on DrrAB-mediated Dox efflux in IOVs. (A) ClustalW alignment of the NBD of DrrA and its prokaryotic or eukaryotic homologs. The conserved motifs present in the NBD are marked at the top. **A.1**, alignment of the NBD of DrrA with proteins (MalK, Sav1866, HlyB, TAP1, TAP2, LmrC, LmrD and LmrA) from diverse ABC families. **A.2**, alignment of the NBD of DrrA with close prokaryotic homologs (belonging to the DRA family/DRR subfamily) (16) identified by NCBI BLAST. **A.3**, alignment of the NBD of DrrA with close eukaryotic homologs belonging to the DRA family/ABCA subfamily (16). **(B) Effect of point mutations in Walker A, Walker B, or the Signature motif of DrrA on DrrAB-mediated Dox efflux in IOVs.** *E. coli* LE392Δ*uncIC* cells containing either pSU2718 vector, pDX101 (*drr*AB in pSU2718), pDX102 (*drr*A only, in pSU2718), pDX103 (*drr*B only, in pSU2718**)** or pDX101 containing mutations of Walker A (G44A, G44S, K47R), Signature motif (S141R), or the Walker B region (E165Q) were induced with IPTG, and the IOVs were prepared, as described under Methods. The initial rate of Dox efflux was determined for each sample, and the relative slopes were calculated, as described for Fig. 1. The average data obtained from three independent experiments are shown in the histogram. **(C) Effect of point mutations in the Switch motif of DrrA on DrrAB-mediated Dox efflux in IOVs.** *E. coli* LE392Δ*uncIC* cells containing either pSU2718 vector, pDX101 (*drr*AB in pSU2718), or pDX101 with mutations of the Walker B region (E165Q) or the Switch motif (Q197H, Y198R, Q197H/Y198H, Q197H/Y198R) were induced with IPTG, and the IOVs were prepared, as described under Methods. The initial rate of Dox efflux was determined for each sample, and the relative slopes were calculated, as described for Fig. 1. The data presented are averages of three independent experiments. Error bars represent standard deviation. **(D) Effect of point mutations in the Switch motif of DrrA on DrrAB-mediated ATPase activity in IOVs.** IOV samples from Fig. 2(C) were subjected to the NADH-coupled ATPase activity assay, as described under Methods. The relative ATPase activity of each sample was obtained by dividing the activity of each sample by the activity of wild type. The data presented are averages of two independent experiments. Error bars represent standard deviation. **(E) Summary of the ATPase activity and Dox efflux activity of wild type DrrAB and Switch motif mutants.**

FIGURE 3. Inhibition of the DrrAB-mediated Dox efflux by known MDR substrates. Dox efflux was measured using 250 µg IOVs in the presence 1 µM Dox and increasing concentrations of the inhibitory substrate in 3ml PBS, pH 7.5. The initial linear rate (100 s - 200 s) of Dox efflux was determined after addition of 1mM ATP/Mg^{2+}. The slope of the efflux curve obtained at 0 concentration of inhibitor was designated as 1.0. The relative slope of each curve was then determined. The average slopes resulting from three independent repeats were plotted by Sigma Plot software using 'scatter plot with error bars', and IC_{50} values were determined. **(A) Kinetic analysis of the inhibitory effect of H 33342 on Dox efflux activity.** The experimental conditions were the same as described above. The assay was carried out in the presence of increasing concentrations of H 33342 ranging from 0 – 1.6 µM. **(B) Kinetic analysis of the inhibitory effect of verapamil.** The experimental conditions were the same as for Fig. 3(A), except that the concentration of verapamil ranged from 0 µM to 100 µM. **(C) Kinetic analysis of the inhibitory effect of Rifampicin.** The experimental conditions were the same as for Fig. 3(A), except that the concentration of rifampicin ranged from 0 µM to 75 µM. **(D) A table showing summary of the IC_{50} values.** Kinetic analysis of the inhibitory effect of various drugs on DrrAB-mediated *in vitro* Dox efflux was determined, as described above for panels 3A-C. The IC_{50} values were calculated as described under Methods.

FIGURE 4. Kinetic characterization of the inhibition of DrrAB-mediated Dox efflux by H 33342, verapamil or rifampicin. The kinetics of DrrAB-mediated Dox efflux was determined in the presence of fixed concentrations of inhibitor, as shown in panels 4A-C. **(A) Competitive inhibition by H 33342.** DrrAB-mediated Dox efflux was studied at four different concentrations of Dox (0.25, 0.5, 0.75 and 1.0

μM) in the presence of a fixed concentration of H33342. In total, four different concentrations of H 33342 (0, 0.2, 0.6, 0.8 μM) were studied. The rate of Dox transport obtained with 1 μM Dox and 0 μM H 33342 was designated as 1.0. The relative rates were then calculated for each efflux curve, and the data were plotted by Lineweaver-Burk plot using Sigma Plot- Kinetics software in Single Substrate – Single Inhibitor Kinetics Format. The error bars represent three separate experiments. The type of inhibition was determined based on the rank of both AICc and R^2. **(B) Non-competitive inhibition by verapamil.** The experiment was performed as described under panel (A). Four different concentrations of verapamil (0, 3.5,7, 14 μM) were used. **(C) Competitive inhibition by rifampicin.** The experiment was performed as described under panel (A). Four different concentrations of rifampicin (0, 5, 10, 20 μM) were used. **(D) Summary of the kinetics constants obtained for inhibition of Dox efflux byH 33342, verapamil and rifampicin.**

FIGURE 5. The DrrAB system forms a multidrug transporter. (A.1) DrrAB-mediated H 33342 efflux in IOVs. The *E. coli* inside-out membrane vesicles were prepared, as described under Methods. 250 μg IOVs were mixed with 0.5 μM H 33342, 0.1 mg/ml creatine kinase and 5 mM creatine phosphate in 3ml PBS buffer, pH 7.4. The fluorescence spectra were recorded on an Alphascan-2-spectrofluorometer with excitation of 355 nm and emission of 457 nm. After 100 s, the detection was paused, and 1mM Mg^{2+} and 1mM ATP, pH 7.5 were added into the reaction. The detection was continued for additional 250 s. Vector, IOVs prepared from cells containing empty vector; DrrAB, IOVs prepared from cells expressing DrrAB. **(A.2) Kinetic analysis of DrrAB-mediated H 33342 efflux in IOVs.** The experimental conditions were the same as described under A.1 above. However, H 33342 efflux was analyzed at concentrations ranging between 0.1 μM to 2.5 μM. The initial (between 100 s-200 s) linear rate of H 33342 efflux was determined. The data obtained from three independent experiments were fitted by the Michaelis-Menten equation using Sigma Plot – Kinetics software in Single Substrate Kinetics Format. **(B.1) DrrAB-mediated EtBr efflux in *E. coli* cells.** *E. coli* cells containing empty vector or DrrAB were loaded with 25 μM EtBr for 1 hr at 37 °C. Energy was provided in the form of 20 mM glucose, and EtBr efflux was measured, as described under Methods. **(B.2) Kinetic analysis of DrrAB-mediated EtBr Efflux in *E. coli* cells.** The experimental conditions were the same as described under B.1 above. However, EtBr efflux was analyzed at concentrations ranging between 1 μM to 100 μM. The steady-state linear rate of EtBr efflux was determined. The data obtained from three independent experiments were fitted by the Michaelis-Menten equation using Sigma Plot – Kinetics software in Single Substrate Kinetics Format. **(C) Summary of the kinetic parameters obtained by using Michaelis-Menten or Hill equation for DrrAB-mediated Dox, H33342, and EtBr efflux.**

TABLE 1. ***Bacterial strain and plasmids***

Name	Description	Reference
	Bacterial Strains or Plasmid	
LE392 Δ*uncIC*	*supE44 supF58 hsdR514 galK2 galT22 metB1 trpR55 lacY1 Δ uncIC*	(22)
pSU2718	Cloning vector, pACYC184 derivative, Cm^r	(17)
pDX101	*drrAB* in pSU2718, Cm^r	(17)
pDX102	*drrA* in pSU2718, Cm^r	(17)
pDX103	*drrB* in pSU2718, Cm^r	(17)
pDX101(G44A)	*drrAB* in pSU2718 with mutation of Gly^{44} to Ala^{44} in the Walker A domain of *drrA*	(31)
pDX101(G44S)	*drrAB* in pSU2718 with mutation of Gly^{44} to Ser^{44} in the Walker A domain of *drrA*	(31)
pDX101(K47R)	*drrAB* in pSU2718 with mutation of Lys^{47} to Arg^{47} in the Walker A domain of *drrA*	(31)
pDX101(S141R)	*drrAB* in pSU2718 with mutation of Ser^{141} to Arg^{141} in the Signature domain of *drrA*	(31)
pDX101(E165Q)	*drrAB* in pSU2718 with mutation of Glu^{165} to Gln^{165} in the Walker B domain of *drrA*	(31)
pDX101(Q197H)	*drrAB* in pSU2718 with mutation of Gln^{197} to His^{197} in the switch motif of *drrA*	This study
pDX101(Y198R)	*drrAB* in pSU2718 with mutation of Tyr^{198} to Arg^{198} in the switch motif of *drrA*	This study
pDX101(Q197H/Y198R)	*drrAB* in pSU2718 with mutation of Gln^{197} Tyr^{198} to His^{197} Arg^{198} in the switch motif of *drrA*	This study
pDX101(Q197H/Y198H)	*drrAB* in pSU2718 with mutation of Gln^{197} Tyr^{198} to $His^{197}His^{198}$ in the switch motif of *drrA*	This study

FIGURE 1

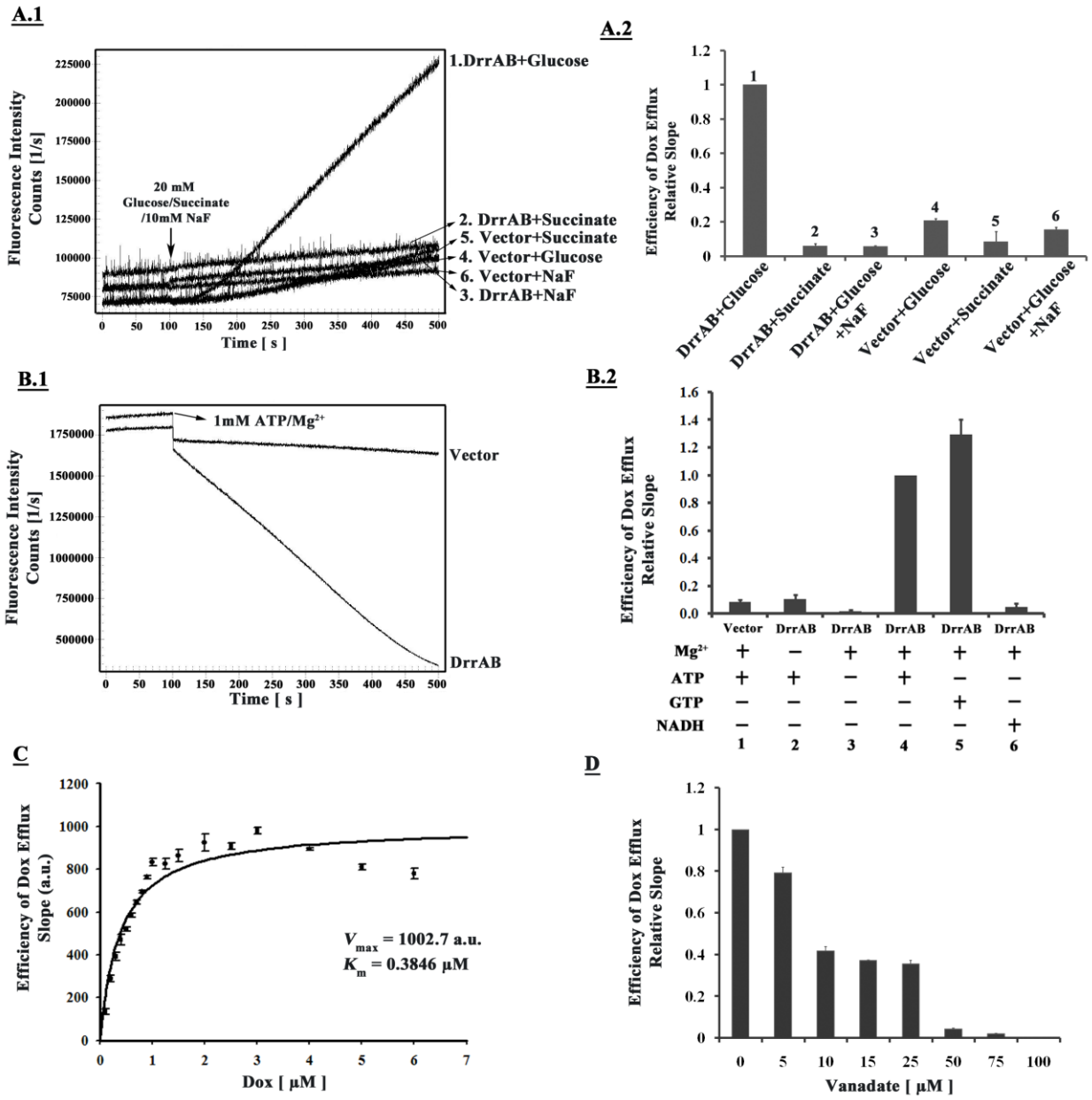

Figure 2

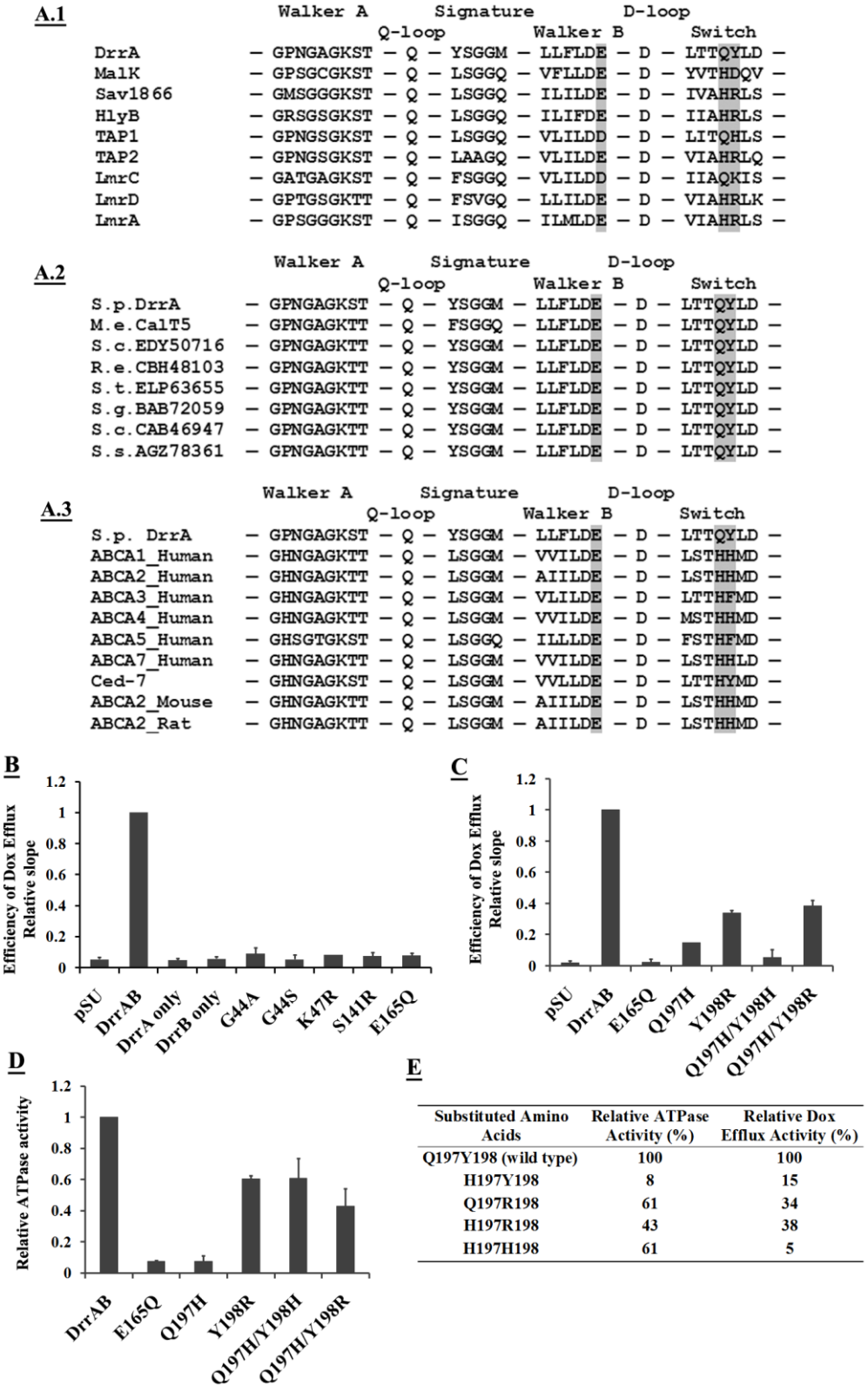

E

Substituted Amino Acids	Relative ATPase Activity (%)	Relative Dox Efflux Activity (%)
Q197Y198 (wild type)	100	100
H197Y198	8	15
Q197R198	61	34
H197R198	43	38
H197H198	61	5

FIGURE 3

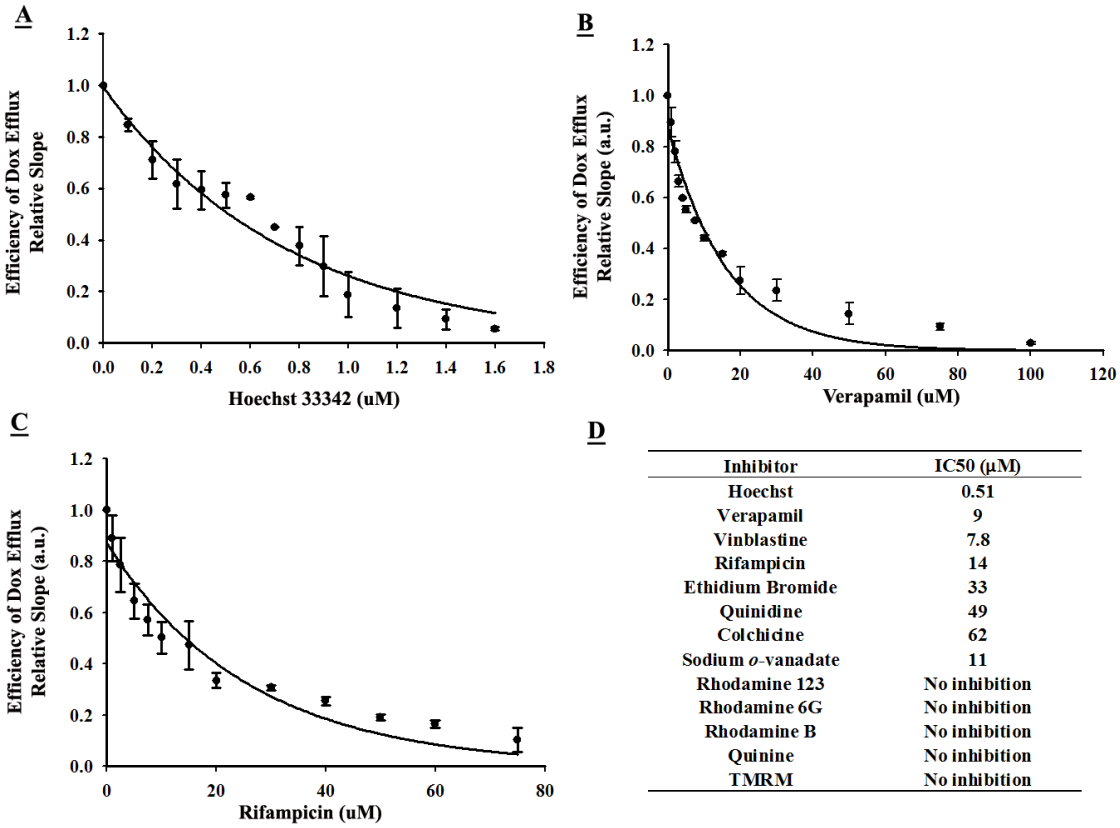

D

Inhibitor	IC50 (μM)
Hoechst	0.51
Verapamil	9
Vinblastine	7.8
Rifampicin	14
Ethidium Bromide	33
Quinidine	49
Colchicine	62
Sodium *o*-vanadate	11
Rhodamine 123	No inhibition
Rhodamine 6G	No inhibition
Rhodamine B	No inhibition
Quinine	No inhibition
TMRM	No inhibition

FIGURE 4

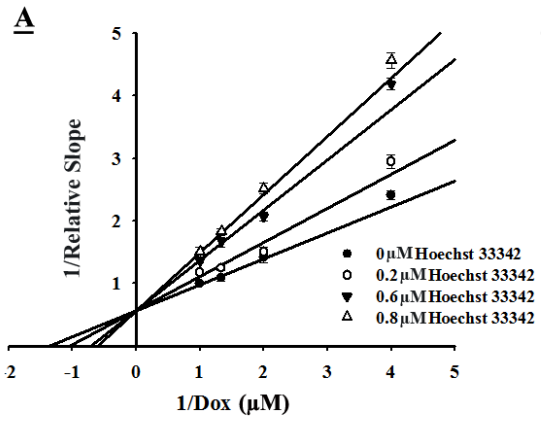

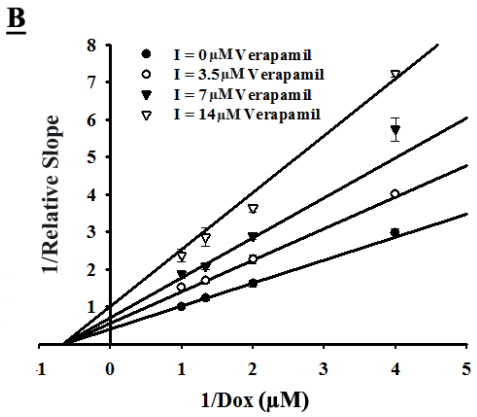

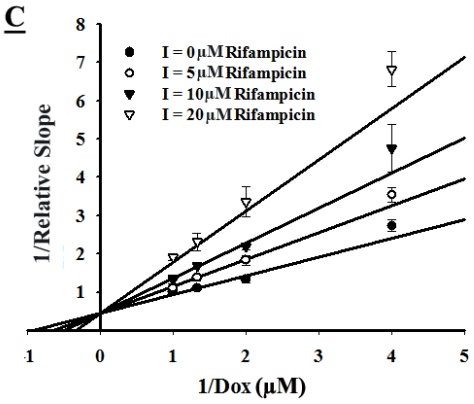

D

Inhibitor	K_i (μM)	Type of inhibition
Hoechst 33342	0.6	Competitive
Verapamil	9.4	Non-competitive
Rifampicin	12	Competitive

FIGURE 5

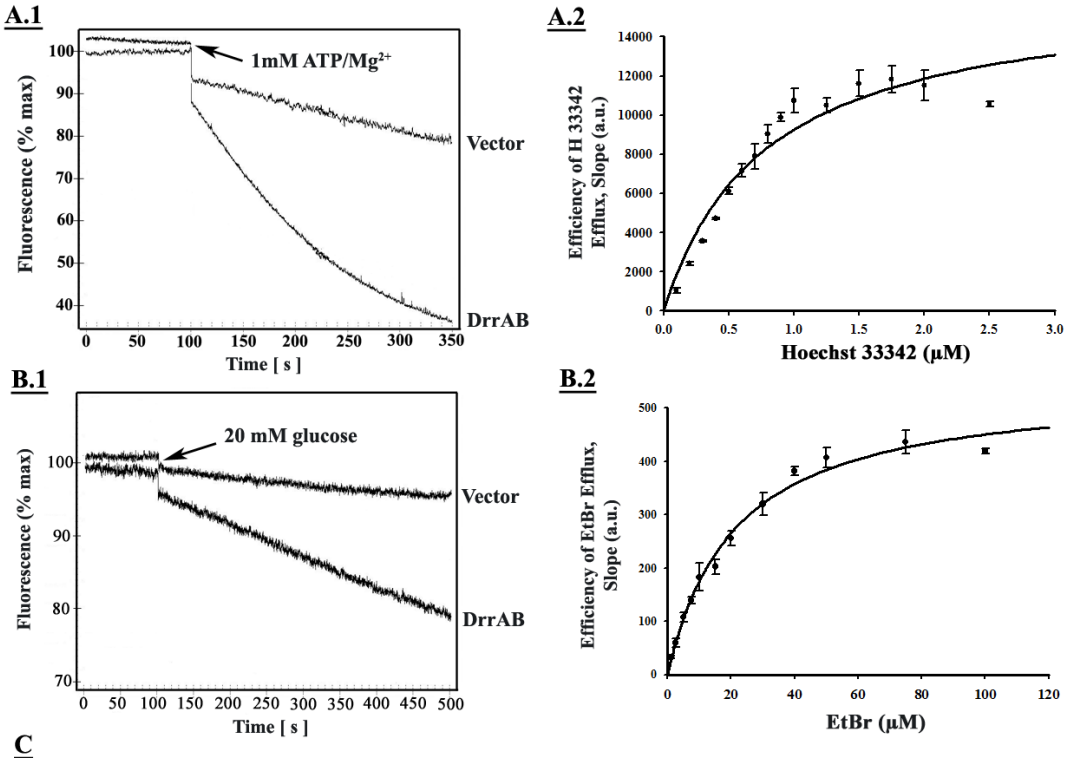

C

Type of Curve	Parameters	Dox	H 33342	EtBr
Michaelis Menten Equation	K_m (μM)	0.39	0.78	21
	V_{max} (a.u.)	1000	16000	550
	R^2	0.89	0.9	0.97
Hill Equation	K_m (μM)	0.36	0.48	19
	V_{max} (a.u.)	910	12000	520
	R^2	0.93	0.95	0.98
	n_{Hill}	1.7	2	1.1

The DrrAB system of Streptomyces peucetius is a Multi-Drug Transporter of Broad Substrate Specificity

Wen Li, Madhu Sharma and Parjit Kaur

J. Biol. Chem. published online March 14, 2014
